APL Electronic Devices

RESEARCH ARTICLE | MARCH 12 2025

# Impact of magnetic ion substitution on the crystal structure of multiferroic Aurivillius phases

Jennifer Halpin ; Michael Schmidt ; Roger W. Whatmore ; Lynette Keeney

Check for updates

*APL Electronic Devices* 1, 016104 (2025)
https://doi.org/10.1063/5.0246803

View Online
Export Citation

## Articles You May Be Interested In

Determination of the thermal conductivity tensor of the $n = 7$ Aurivillius phase $Sr_4Bi_4Ti_7O_{24}$

*Appl. Phys. Lett.* (July 2012)

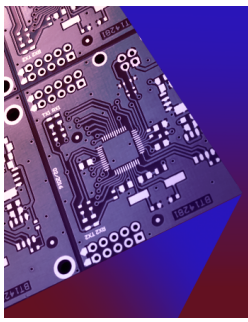
Coexisting magnetic orders and concomitant Morin-like transition and relaxor behavior in multiferroic Aurivillius $Bi_4Ti_{3-2x}Nb_xFe_xO_{12}$ compounds

*Appl. Phys. Lett.* (September 2022)

Magnetic-field-induced ferroelectric domain dynamics and in-plane polarization in odd and mixed layered Aurivillius structures

*J. Appl. Phys.* (August 2019)

04 August 2025 15:15:43



APL Electronic Devices
Fostering connections across multiple disciplines in the broad electronics community
Now Open for Submissions
AIP Publishing

AIP Publishing

APL Electronic Devices ARTICLE pubs.aip.org/aip/aed

# Impact of magnetic ion substitution on the crystal structure of multiferroic Aurivillius phases

Cite as: APL Electron. Devices 1, 016104 (2025); doi: 10.1063/5.0246803
Submitted: 4 November 2024 • Accepted: 19 January 2025 •
Published Online: 12 March 2025

View Online Export Citation CrossMark

Jennifer Halpin,[1] Michael Schmidt,[1] Roger W. Whatmore,[2,3] and Lynette Keeney[1,a)]

## AFFILIATIONS

[1] Tyndall National Institute, University College Cork, "Lee Maltings Complex," Dyke Parade, Cork T12 R5CP, Ireland
[2] School of Chemistry, University College Cork, Cork, Ireland
[3] Department of Materials, Faculty of Engineering, Imperial College, London SW7 2AZ, United Kingdom

[a)] **Author to whom correspondence should be addressed:** lynette.keeney@tyndall.ie

## ABSTRACT

The five-layered ($m$ = 5) $Bi_6Ti_{2.99}Fe_{1.46}Mn_{0.55}O_{18}$ Aurivillius material is a rare example of a single-phase room temperature ferroelectric–ferrimagnetic multiferroic that shows promise for energy-efficient memory devices. Its ferrimagnetism is thought to derive from the natural partitioning of magnetic ions to the central perovskite layer, engendered by chemically driven lattice strains, together with ferromagnetic coupling via super-exchange mechanisms. Motivated by the expectation of an enhancement in magnetization with increased magnetic ion content, this study examines systematic B-site substitutions with the aim of increasing (from the current level of 40%) the proportion of magnetic ions within the structure. The solubility limits of magnetic cations in this structure and their influence on the superlattice layering are investigated. The studies of Aurivillius phase films on $c$-sapphire with composition $Bi_6Ti_xFe_yMn_zO_{18}$ (B6TFMO; x = 2.3–3.2, y = 1.2–2.0, z = 0.3–0.9) demonstrated that above ~46% of B-site magnetic cations, the $m$ = 5 structure first rearranges into a mixed-phase material based on $m$ = 5 and six-layered ($m$ = 6) structures and eventually evolves into an $m$ = 6 phase with 54% magnetic cations at the B-site. It is demonstrated that higher-layered Aurivillius homologs can be synthesized using aliovalent substitution, without requiring epitaxial growth or kinetically constrained methods. It is postulated that increasing the number of perovskite layers by forming the $m$ = 6 structure facilitates the accommodation of additional magnetic cations at a lower average manganese oxidation state (+3.3) compared with an equivalent $m$ = 5 stoichiometry (+4.0). While the minor out-of-plane ferroelectric response decreases as expected with increasing structural reorganization toward the $m$ = 6 phase, the predominant in-plane piezoresponse remains unaffected by increased magnetic cation substitution. This work implies possibilities for enhanced magnetic properties in room temperature multiferroic materials, initiating the development of technologically viable ultralow-power multiferroic memory devices.

*© 2025 Author(s). All article content, except where otherwise noted, is licensed under a Creative Commons Attribution (CC BY) license (https://creativecommons.org/licenses/by/4.0/).* https://doi.org/10.1063/5.0246803

04 August 2025 15:15:43

## I. INTRODUCTION

Data storage is a critical enabler to all aspects of modern life. It was estimated that in 2023, digital data storage stood at 64 zettabytes, roughly doubling every two years.[1] Contemporary computer storage technologies use either electric or magnetic polarization to store single bits of information; a power-hungry technology that will soon struggle to keep-up with the ever-increasing demands. Masanet *et al.*[2] pointed out that in 2018, data centers used 205 TWh of electricity, ~1% of global consumption. Interestingly, due to major increases in energy efficiency, this was only a 6% increase on the 2010 figure, despite a 550% increase in digital data storage over the same period. This emphasizes the importance for the sector of maintaining the energy-efficiency trajectory.

The capability of ferroelectrics and ferromagnetic/ferrimagnetic materials to switch their order parameters between two stable states makes them ideal candidates for use as state variables in data storage and computation. Materials that exhibit both ferroelectric and ferromagnetic/ferrimagnetic properties within a single phase are known as multiferroic materials. Multiferroic technologies that simultaneously combine ferroelectric and ferromagnetic/ferrimagnetic properties can use energy-efficient electric fields for the reading and writing of data. (For the rest of this paper, the term "multiferroic" will be used as a shorthand


© Author(s) 2025

for "ferroelectric–ferrimagnetic multiferroic.") Magnetoelectric coupling refers to the induction of magnetization by an electric field, or vice versa, and may arise directly in a single-phase material when the switching of one order parameter (e.g., ferrimagnetic polarization) induces a switching of the other order parameter (e.g., ferroelectric polarization). Devices based on electric-field control of magnetism in magnetoelectric multiferroic architectures offer the potential for ultralow switching energy ($10^{-18}$ J per switch) at ultralow switching voltages (<100 mV). This represents a significant reduction in energy consumption compared to spin-transfer torque devices, which require high current densities to generate magnetic fields and exhibit switching energies of ~$10^{-15}$ J per switch.[3,4] While artificial (composite) magnetoelectrics offer large magnetoelectric coupling values [e.g., magnetoelectric susceptibility ~660 for Ni/Pb($Mg_{0.66}Nb_{0.33}$)$O_3$–$PbTiO_3$][5] and room temperature applications,[6,7] technologies based on single-phase multiferroics offer advantages of intrinsic coupling of ferroic properties, reduced interface issues, and simplified device architectures. The unique potential of single-phase multiferroics lies in enabling multi-state storage devices by leveraging simultaneous electroresistance and magnetoresistance states. When electrons tunnel through an ultrathin multiferroic tunnel junction, this approach could, in-principle, achieve an eightfold increase in data storage capacity per cell relative to conventional binary switches.[8] No such commercial devices exist, however, as the single-phase multiferroic materials needed for this technology are extremely rare at room-temperature. Moreover, enhancing the remanent magnetic moment at room temperature is a critical requirement for developing technologically viable multiferroics suitable for ultralow-power memory devices.[4]

The Aurivillius phase materials are well-established[7,9] layered ferroelectrics, whose general formula is $Bi_2O_2(A_{m-1}B_mO_{3m+1})$, where "$m$" denotes the number of perovskite-type layers interleaved between $[Bi_2O_2]^{2+}$ fluorite layers.[10,11] Ferroelectricity has been shown to persist in exfoliated Aurivillius phase nano-flakes and epitaxial thin films with thicknesses of only ~2 nm.[12–15] This natural superlattice structure offers a versatile framework for designing single-phase multiferroic materials with potential applications in energy-efficient data storage.[16,17] They can incorporate magnetic cations such as Fe, Mn, and Cr at their perovskite B-sites, facilitating magnetic super-exchange interactions.[18–22] The Mn- and Fe-containing $Bi_6Ti_{2.99}Fe_{1.46}Mn_{0.55}O_{18}$ ($m$ = 5) (B6TFMO) Aurivillius phase system with 40% magnetic cations at the B-sites is a rare example of a single-phase room temperature multiferroic, displaying saturation magnetization ($M_S$) values of 215 emu/cm$^3$ and in-plane saturation polarization ($P_s$) values of >26 $\mu$C/cm.[19,20,23] The dual substitution of Mn and Fe into the $Bi_2O_2(Bi_{m-1}Ti_mO_{3m+1})$ structures is key for achieving multiferroic behavior. Notably, ferromagnetism has only been observed in the Mn-only substituted $Bi_2O_2(Bi_{m-1}Ti_mO_{3m+1})$ materials at temperatures below 55 K.[22] In Mn and Fe co-substituted $Bi_6Ti_{2.99}Fe_{1.46}Mn_{0.55}O_{18}$, the presence of Mn promotes ferrimagnetic ordering, in contrast to the negligible magnetization observed in the corresponding Fe-only $Bi_2O_2(Bi_{m-1}Ti_mO_{3m+1})$ analog.[24] Atomic resolution electron microscopy from previous studies[21,24,25] has revealed a natural tendency for magnetic cations, particularly Mn, to concentrate in the central perovskite layer. Density functional theory (DFT) calculations[24,25] show that this magnetic cation partitioning, coupled with the spin states of the magnetic cations, plays an important role in influencing the magnetic exchange interactions and the resulting magnetization values. Furthermore, B6TFMO Aurivillius phase films synthesized by both chemical solution and chemical vapor deposition (CVD) demonstrate the reversible magnetoelectric switching at room temperature necessary for practical energy-efficient magnetoelectric device applications.[19,20]

For technologically competitive devices, a necessary requirement for multiferroic materials is the enhancement of the magnetic properties by means of strongly interacting magnetic moments with long-range spin ordering. Introducing a higher volume of magnetic ions to surpass the percolation threshold[26] is a well-known strategy for enhancing long-range magnetic ordering and magnetization (see Sec. SI1 of the supplementary material). In addition, computational studies on the Aurivillius phases by Birenbaum *et al.*[27] have demonstrated that increasing the concentration of magnetic ions raises the ferrimagnetic Curie temperature. Thus, increasing the magnetic ion concentration at the B-site of the B6TFMO structure beyond the current level of ~40% is a critical factor in further improving its magnetic properties and data storage device performance.

However, the Aurivillius phase structure is expected to have a limit on the concentration of Fe and Mn it can accommodate. One constraint stems from differences in cation radii: when coordinated octahedrally by oxygen, $Ti^{4+}$ has a radius of 0.605 Å, whereas both $Fe^{3+}$ and $Mn^{3+}$ (in their high-spin states) have a radii of 0.645 Å.[28] (NB: The high-spin state is favored for transition metals in Aurivillius phase structures due to structural and electronic factors. These include the large size of bismuth resulting in weakened ligand fields, distortion in the coordination environment due to neighboring layers, and incomplete hybridization between metal $d$ orbitals and ligand orbitals.[29]) Another limitation arises because these cations have a nominal valence of 3+, and they replace $Ti^{4+}$, which has a valence of 4+. Substituting $Ti^{4+}$ by $Mn^{3+}$/$Fe^{3+}$ requires charge compensation, for which several mechanisms can be postulated. One possibility for charge compensation is through changes in the oxidation states (o.s.) of the Mn or Fe cations.[19,30,31] Alternatively, exceeding the solubility limit may lead to the segregation of impurity species or the formation of secondary phases at grain boundaries or surfaces.[32–34] Another potential mechanism is ionic compensation through the introduction of ionic defects such as oxygen vacancies.[31,35,36] However, in Aurivillius phase materials, the $[Bi_2O_2]^{2+}$ layers are recognized for their important role in space charge compensation and prevention of oxygen vacancies, which in turn reduces leakage currents and enhances fatigue resistance in ferroelectric random access memory devices.[37,38]

Given these considerations, to advance the development of reproducible multiferroic materials with enhanced magnetic properties for low-power data storage devices, it is important to understand how increasing the concentration of magnetic ions in $m$ = 5 Aurivillius phases affects the crystal structure. To investigate this, we systematically varied the concentrations of the three B-site atoms (Ti, Fe, and Mn) in the B6TFMO system, $Bi_6Ti_xFe_yMn_zO_{18}$ (x = 2.3–3.2, y = 1.2–2.0, z = 0.3–0.9). This approach enabled us to determine the solubility limit of magnetic ion inclusion in the $m$ = 5 Aurivillius phase structure and assess its impact on the superlattice layering. We consider the above size and charge compensation

04 August 2025 15:15:43


© Author(s) 2025

mechanisms and demonstrate that structural reorganization into higher *m* phases is a further option available to the versatile Aurivillius phase structures to accommodate a greater magnetic ion fraction while preserving in-plane ferroelectric properties. Furthermore, we show that aliovalent substitution using transition metal cations, through simple chemical solution deposition (CSD) processes, can overcome thermodynamic challenges of synthesizing higher-layered Aurivillius homologs without requiring epitaxial substrates or kinetically limited growth processes. Although a comprehensive analysis of phase purity (beyond the scope of the present article) is necessary before reliable magnetometry studies can be conducted, it is anticipated that increasing the magnetic cation content will enhance the magnetic moment and multiferroic properties of the new Aurivillius phase compositions.[19,20,23,33,34]

## II. EXPERIMENTAL METHODS

Chemical solution deposition (CSD) was used to fabricate the $Bi_6Ti_xFe_yMn_zO_{18}$ compositions as thin films[19] (see Sec. SI2 of the supplementary material). The average film thickness, as determined by transmission electron microscopy (TEM), was 89 nm (standard deviation 33 nm across 265 measurement points). The general formulas of the different series were as follows: series 1: $Bi_6Ti_3Fe_{1.6-\alpha}Mn_{0.4+\alpha}O_{18}$ ($\alpha$ = 0, 0.1, 0.2, 0.3, and 0.4), series 2: $Bi_6Ti_{3.2-\beta}Fe_{1.5}Mn_{0.3+\beta}O_{18}$ ($\beta$ = 0, 0.1, 0.2, 0.3, 0.4, 0.5, and 0.6), series 3: $Bi_6Ti_{3.2-\gamma}Fe_{1.3+\gamma}Mn_{0.5}O_{18}$ ($\gamma$ = 0, 0.1, 0.2, 0.3, 0.4, 0.5, and 0.6), and series 4: $Bi_6Ti_xFe_yMn_zO_{18}$ (x = 2.3–2.8, y = 1.52–2.00, z = 0.68–0.75).

X-ray diffraction measurements (XRD) were performed using a Philips X'pert PW3719 MPD diffractometer, Cu K$\alpha$ radiation, 40 kV, 35 mA, and 2$\theta$ range of 6°–40°. The *m* = 4 Aurivillius phase was indexed from calculated XRD patterns generated using the CrystalDiffract 7 software (CrystalMaker Software Ltd.) using data from Hervoches *et al.*[39] The *m* = 5 Aurivillius phase was indexed from calculated XRD patterns generated using the CrystalDiffract 7 software (CrystalMaker Software Ltd.) using data modified from García-Guaderrama *et al.*[40] The *m* = 6 phase was indexed from calculated XRD patterns generated using the CrystalDiffract 7 software (CrystalMaker Software Ltd.) using data modified from Krzhizhanovskaya *et al.*[41] CrystalDiffract® is a powder diffraction program for Mac and Windows, CrystalMaker Software Ltd., Oxford, England (www.crystalmaker.com). Refer to Sec. SI4.1 of the supplementary material for further details. Atomistic structural models of the modified *m* = 5 and *m* = 6 structures were generated using VESTA.[42]

Atomic Force Microscopy (AFM) and Piezo-Force Microscopy (PFM) measurements and ferroelectric lithography experiments were performed using an MFP-3D™ Asylum Research instrument (see Sec. SI2 of the supplementary material for details).

Scanning electron microscopy (SEM) was performed on a Zeiss SUPRA 40 instrument, and the samples were treated with a 3–6 nm thickness gold coating before measurement to prevent charging during imaging. Lamella cross sections of the films were prepared using a FEI DualBeam Helios NanoLab 600i Focused Ion Beam instrument. High resolution transmission electron microscopy (HR-TEM) was performed using a JEOL 2100 transmission electron microscope, 200 kV, double tilt holder. Note that normally ~10% error should be accounted for when calculating distances from TEM data due to the electron optics of the instrumentation. Composition analysis was conducted using high-resolution scanning transmission electron microscopy (STEM) and energy dispersive x-ray spectroscopy (EDX) equipped with an X-Max 80 detector and the AZtec analysis software (Oxford Instruments, Abingdon, UK).

## III. RESULTS

### A. Structural investigations of B-site substitution within the B6TFMO Aurivillius phases

#### 1. XRD analysis

The concentrations of two of the three types of B-site cations were systematically varied within the B6TFMO series 1, 2, and 3, while the third cation concentration was kept constant. XRD analysis (Fig. SI1) of series 1 was overall consistent with an *m* = 5 Aurivillius phase structure. In this section, we will examine what factors influence deviations from this.

For series 1 [$Bi_6Ti_3Fe_{1.6-\alpha}Mn_{0.4+\alpha}O_{18}$ ($\alpha$ = 0, 0.1, 0.2, 0.3, and 0.4)], the concentrations of Fe and Mn are varied, while Ti concentration remains constant. In other words, the Ti:Mn/Fe stoichiometric ratio of 3:2 does not change across series 1. This was considered isovalent substitution since both Fe and Mn are nominally in the 3+ oxidation state (o.s.) in a neutral B6TFMO Aurivillius stoichiometry. They also have similar ionic radii as noted above,[28] although it is acknowledged that the Jahn–Teller effect can tend to elongate $Mn^{3+}O_6$ octahedra.[43] The XRD plots of sample series 1 shown in Fig. SI1 show that the peak positions, heights, and widths correlate well with a computed XRD diffraction pattern for a refinement of a reference *m* = 5 structure[40] shown in the supplementary material, Sec. SI4.1, Fig. SI2. The reference pattern is computed with an assumed 90% preferred crystallite (00*l*) orientation, a nominal crystal size of 30 nm, and an isotropic strain of 0.1%, to give a line breadth similar to that observed in the *m* = 5 phase in Fig. SI1. The 30 nm crystallite size inferred from XRD analysis is between 0.5 and 0.3 that of the observed crystallite thickness in cross section TEM as shown in Figs. 1(c) and 1(e), an observation that is probably indicative that the crystallite coherence due to structural disorder is significantly smaller than the film thickness. As the concentration of Mn increases and Fe decreases, there is only a slight shift (~0.4°) in 2$\theta$ peak positions accompanied by peak broadening. For example, the (00$\bar{1}$0) peak full width half maximum (FWHM) is 0.45° for $\alpha$ = 0 and is 0.50° for $\alpha$ = 0.4 ($Bi_6Ti_3Fe_{1.6-\alpha}Mn_{0.4+\alpha}O_{18}$). This probably indicates increasing structural disorder within the samples, such as the formation of out-of-phase boundary (OPB) defects, which are common to the Aurivillius structures.[21,24,44–46] Evidence for these is presented in Sec. III A 2.

The Aurivillius phase structure is highly anisotropic, and the films show strongly preferred *c*-axis orientation, as is evidenced by the majority of XRD peaks displaying (00*l*) reflections. The pseudo-lattice parameter of the perovskite-type layer ($a_p'$) in B6TFMO (3.89 Å)[45] differs significantly from the lattice constant of sapphire (a = 4.785 Å), resulting in a +22.97% lattice mismatch. Consequently, there is no epitaxial relationship with the substrate, and the films grow without strain. The *c*-orientation arises naturally from the inherent layering and anisotropy of the Aurivillius phase,

04 August 2025 15:15:43


© Author(s) 2025

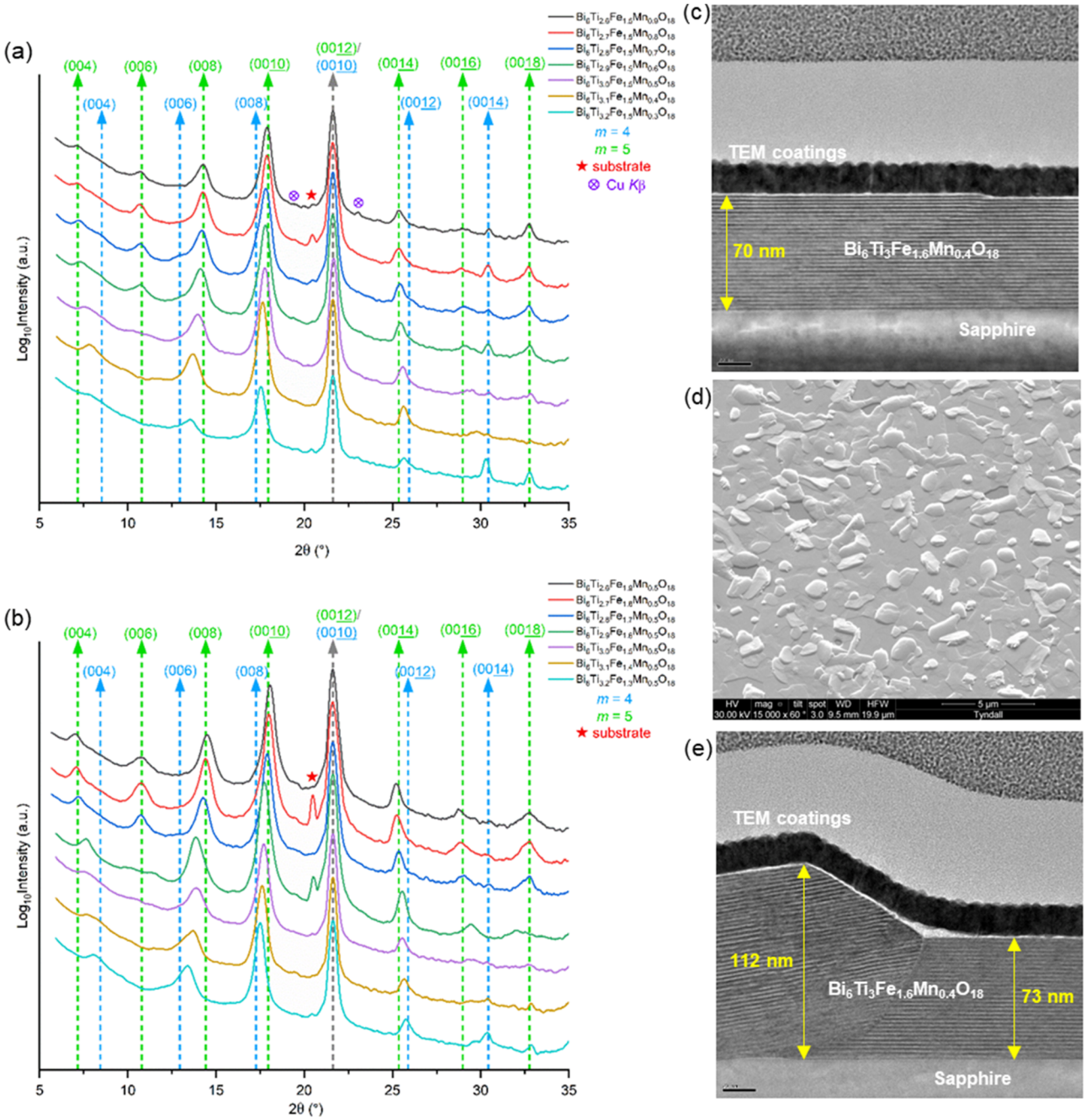



**FIG. 1.** XRD analysis of (a) series 2 and (b) series 3. (c) TEM, (d) SEM, and (e) TEM images of the $Bi_6Ti_3Fe_{1.6}Mn_{0.4}O_{18}$ sample from series 1 confirm the layered and plate-like Aurivillius phase $m = 5$ structure.

rather than from epitaxial effects. TEM images [Fig. 1(c)] of samples from series 1 confirm the layered $m = 5$ structure and verify the preferential growth of grains in directions normal to the stacking axis ($c$-axis) of the layers. The grains crystallize with plate-like morphology with in-plane grain size ranging from 10 nm to 2 $\mu$m [Fig. 1(d)]. Lamellar-type growth is commonly observed in ceramic samples and the non-epitaxial films of Aurivillius phases, characterized by anisotropic, plate-like crystals arranged in a layered structure.[33,47] This growth occurs due to the high grain growth rate perpendicular to the $c$-axis, driven by the lower surface energy

04 August 2025 15:15:43


© Author(s) 2025

of the (001) planes.[48] The crystallites overlap one another at grain boundaries [Fig. 1(e)], meaning that thickness variation (typically 89 ± 33 nm) is observed across the samples, with rms roughness ranging from 16 to 27 nm.

Although Li *et al.*[49] reported a slight increase in grain size in Mn-substituted $Bi_5Ti_3Fe_1O_{15}$, no clear effect on the morphology was observed in this work with the substitution of Fe by Mn. The XRD and TEM data illustrate that isovalent substitution of Fe by Mn in series 1 does not lead to any structural rearrangements.

Series 2 [$Bi_6Ti_{3.2-\beta}Fe_{1.5}Mn_{0.3+\beta}O_{18}$ (β = 0, 0.1, 0.2, 0.3, 0.4, 0.5, and 0.6)] involves the substitution of Ti for Mn and is an example of aliovalent substitution since Ti has a nominal valence of 4+, while the Mn precursor used has a nominal valence of 3+, although it can oxidize to 4+ under oxidizing conditions or reduce to 2+ under reducing conditions.[21] For β = 0 and 0.1, there $Ti^{4+}$ concentration is increased, necessitating charge compensation through a reduction in the oxidation states of the Mn or Fe cations. Conversely, for β = 0.3 to 0.6, $Ti^{4+}$ concentration is decreased, requiring charge compensation via an increase in the oxidation states of the Mn or Fe cations. It is evident from the XRD analysis of series 2 [Fig. 1(a)] that as the Ti content decreases and the Mn content increases, there is a clear gradual shift in peak position away from a mixed $m$ = 4 and $m$ = 5 phase sample and toward a single $m$ = 5 Aurivillius phase. As β increases from 0 to 0.6, the 2θ position of the (008) reflection shifts from 13.6° to 14.4° and the position of the (00$\underline{1}$0) reflection shifts from 17.6° to 18.0°, corresponding to the expected positions for the (008) and (00$\underline{1}$0) for an $m$ = 5 structure. A similar trend in asymmetric peak shift on aliovalent substitution is observed in series 3 [$Bi_6Ti_{3.2-\gamma}Fe_{1.3+\gamma}Mn_{0.5}O_{18}$ (γ = 0, 0.1, 0.2, 0.3, 0.4, 0.5, and 0.6), Fig. 1(b)], where the B-site concentration of Ti is decreased and the concentration of Fe is increased. For example, as γ increases from 0 to 0.6, the 2θ position of the (008) reflection moves from 13.4° to 14.5° and the position of the (00$\underline{1}$0) reflection moves from 17.5° to 18.1°, corresponding to a pure $m$ = 5 phase.

In series 4 [$Bi_6Ti_xFe_yMn_zO_{18}$ (x = 2.3–2.8, y = 1.52–2.00, z = 0.68–0.75)], the concentration of Ti was further reduced. The compositions were selected based on a compositional survey of 55 individual Aurivillius phase grains from a previous study of a mixed $m$ phase B6TFMO sample.[19] This series explores the aliovalent substitution of Ti by both Mn and Fe, allowing x, y, and z to vary within the series. XRD data for series 4 are presented in Fig. 2(a), while AFM images showing the surface morphology of compositions $Bi_6Ti_{2.6}Fe_{1.72}Mn_{0.68}O_{18}$ and $Bi_6Ti_{2.3}Fe_{1.95}Mn_{0.70}O_{18}$ are shown in Figs. 2(b) and 2(c), respectively.

As the Ti concentration decreases and Fe and Mn increase, the XRD patterns [Fig. 2(a)] clearly demonstrate a shift from a pure $m$ = 5 phase [in $Bi_6Ti_{2.8}Fe_{1.52}Mn_{0.68}O_{18}$ and $Bi_6Ti_{2.7}Fe_{1.62}Mn_{0.68}O_{18}$ (see the supplementary material, Sec. SI4 and Figs. SI2 and SI4)] to a sample with a significant $m$ = 6 presence. This transition is evident as $x$ decreases from 2.8 to 2.3, with the intensities of the (006), (008), (00$\underline{1}$0), (00$\underline{1}$4), (00$\underline{1}$6), and (00$\underline{1}$8) reflections of the $m$ = 5 phase

04 August 2025 15:15:43

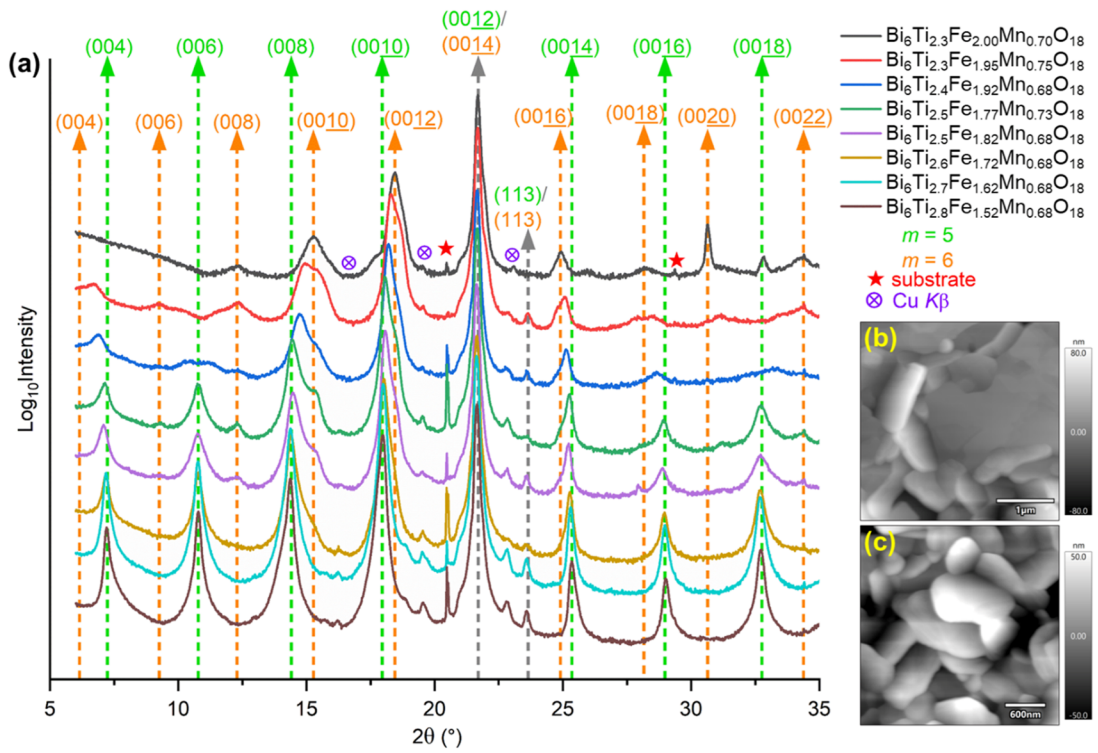



**FIG. 2.** (a) XRD analysis of series 4. AFM images of the surface morphology for compositions (b) $Bi_6Ti_{2.6}Fe_{1.72}Mn_{0.68}O_{18}$ and (c) $Bi_6Ti_{2.3}Fe_{1.95}Mn_{0.70}O_{18}$ demonstrate how grains crystallize with plate-like morphology.


© Author(s) 2025

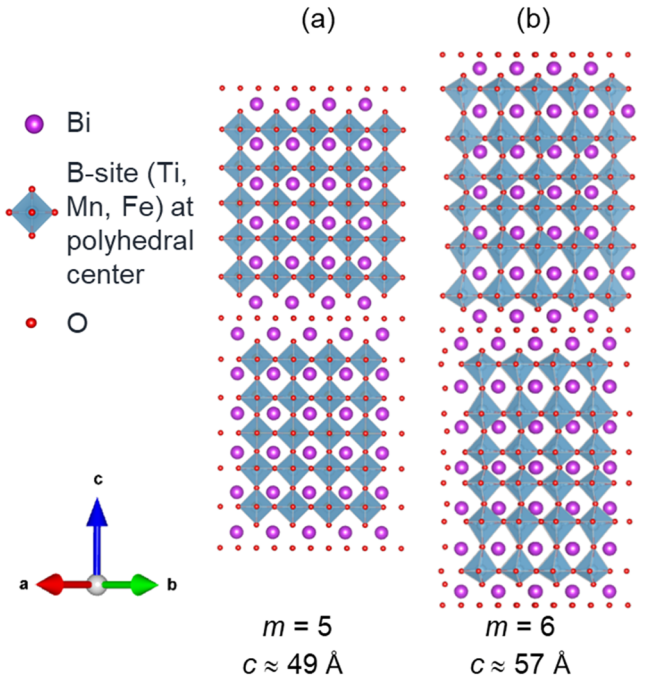



**FIG. 3.** Atomistic structures of one unit cell of Aurivillius phases. (a) $m = 5$ structure and (b) $m = 6$ structure.

gradually diminishing [e.g., the intensity of the (006) reflection drops from 38 951 to 116 counts]. Concurrently, peaks associated with the (008), (0010), (0012), (0016), (0018), and (0020) reflections of the $m = 6$ phase begin to emerge, especially when the Ti concentration falls below 2.5 at the B-site. Figure 3 shows the simulated atomistic structures of one unit cell for a five layered structure (based on modified data from García-Guaderrama *et al.*;[40] see SI.4.1) and a six layered structure (based on modified data from Krzhizhanovskaya *et al.*;[41] see SI.4.1). It is important to note that these structures were not investigated with the aim of achieving complete crystal structure refinements. The available XRD data are insufficient for a full structural analysis or an accurate characterization of octahedral tilting and distortions. However, the simulated models serve the purpose of estimating changes in the relative concentrations of the $m = 5$ and $m = 6$ phases within the XRD patterns shown in Fig. 2(a).

The XRD patterns of $Bi_6Ti_{2.6}Fe_{1.72}Mn_{0.68}O_{18}$, $Bi_6Ti_{2.5}Fe_{1.82}Mn_{0.68}O_{18}$, $Bi_6Ti_{2.5}Fe_{1.77}Mn_{0.73}O_{18}$, $Bi_6Ti_{2.4}Fe_{1.92}Mn_{0.68}O_{18}$, and $Bi_6Ti_{2.3}Fe_{1.95}Mn_{0.75}O_{18}$ align well with computed XRD diffraction patterns refined for samples containing a mix of $m = 5$ and $m = 6$ structural phases, as detailed in the supplementary material, Sec. SI4.2 and Figs. SI5 and SI6. Although small regions within the samples may exhibit random intergrowth of $m = 5$ and $m = 6$ blocks, the XRD modeling confirms that these are primarily distinct phases, not an $m = 5.5$ phase ($c \approx 53$ Å) formed by recurring intergrowth of $m = 5$ and $m = 6$ Aurivillius half-unit cells.[50] For instance, the $Bi_6Ti_{2.3}Fe_{1.95}Mn_{0.75}O_{18}$ sample is composed of 70% distinct $m = 5$ phase ($c \approx 49$ Å) [Fig. 3(a)] and 30% distinct $m = 6$ phase ($c \approx 57$ Å) [Fig. 3(b)].

The XRD pattern for $Bi_6Ti_{2.3}Fe_{2.0}Mn_{0.7}O_{18}$, with the lowest Ti content of the samples investigated, predominantly exhibits $m = 6$ characteristics, closely matching a simulated pattern for a refined reference model, as discussed in Sec. SI4.1 and shown in Fig. SI3 of the supplementary material. A summary of the results from the two-phase XRD modeling results is provided in Table I, showing a clear trend toward the structural evolution of higher-layered Aurivillius phases to accommodate increased magnetic cation substitution.

The full width half maximum (FWHM) values of the XRD peaks for the $m = 5$ phase increase as the Ti concentration decreases across Series 4 (see Table I). While particle size effects could contribute to peak broadening,[51] the consistent deposition method applied throughout the series should limit significant variations in film thickness and grain size. In addition, XRD pattern modeling (see Sec. SI4 of the supplementary material) indicates that no single crystallite size can fully account for the broadening observed in all reflections, as the peaks widen independently of crystal size. Increased structural stacking disorder, such as stacking faults, OPB defects, and small regions of phases with different $m$ values (evident in the TEM data in Fig. 4), almost certainly contributes to the broadening of the XRD peaks,[44,52–55] which is reflected in the FWHM values. The increase in peak broadening for the $m = 5$ phase implies a more disordered periodic structure as $x$ values decrease. Furthermore, peak broadening for the $m = 6$ phase is over twice that of the $m = 5$ reflections at the same 2 theta value, indicating that the $m = 6$ phase is more defective than the $m = 5$ phase.

The shift to the higher $m = 6$ Aurivillius phase is interesting, given that access to larger layering periods is constrained by thermodynamics. The difference in formation enthalpy between different $m$-phases of similar composition is often too subtle to stabilize one phase relative to another;[56] therefore, it appears that the chemical modifications are responsible for stabilizing the formation of the higher $m$-Aurivillius phase.

### 2. Electron microscopy analysis

TEM analysis (Fig. 4) confirmed the increased structural rearrangement to $m = 6$ layered units as the Ti content within the films decreases. The thickness of a unit cell along the growth ($c$) axis of the Aurivillius structure can be estimated using the formula $c/2 = f + h$, where $h = m * p.f$ refers to the thickness of the $[Bi_2O_2]^{2+}$ interlayer, which is estimated to be 4.08 Å.[57] The average thickness of the perovskite blocks ($p$) is ≈4.11 Å, and $m$ refers to the number of perovskite blocks per half-unit cell of the Aurivillius phase structure.[57] Thus, $c$ is calculated to be 41.04 Å for an $m = 4$ structure, 49.26 Å for an $m = 5$ structure, and 57.48 Å for an $m = 6$ structure. This correlates well with the $c$-axis lattice parameters in the literature physically determined by x-ray and powder neutron diffraction data.[19,39,41,58]

TEM imaging supports the XRD findings that the $Bi_6Ti_{2.8}Fe_{1.52}Mn_{0.68}O_{18}$ composition is primarily structured as the $m = 5$ phase, with a measured $c$-axis length of 4.6 ± 0.1 nm, which is within 10% instrumental error of the expected 4.9 nm [Fig. 4(a)]. As the Ti content decreases, TEM images reveal an increasing presence of mixed $m = 5$ and $m = 6$ phases. TEM imaging of the $Bi_6Ti_{2.3}Fe_{1.95}Mn_{0.75}O_{18}$ composition [Fig. 4(c)] corroborates XRD observations [Fig. 2(a) and Table I], confirming a distinct

04 August 2025 15:15:43


© Author(s) 2025

**TABLE I.** Comparison of experimental XRD data in Fig. 2(a) with the predicted XRD patterns.

| Composition | % age m = 5 | % age m = 6 | (00$\underline{10}$) FWHM$_q$ m = 5 (°) | (00$\underline{12}$) FWHM$_q$ m = 6 (°) | c-axis m = 5 (Å) | c-axis m = 6 (Å) |
|---|---|---|---|---|---|---|
| $Bi_6Ti_{2.8}Fe_{1.52}Mn_{0.68}O_{18}$ | 100 | 0 | 0.117 | ⋯ | 49.29 | ⋯ |
| $Bi_6Ti_{2.7}Fe_{1.62}Mn_{0.68}O_{18}$ | 100 | 0 | 0.121 | ⋯ | 49.29 | ⋯ |
| $Bi_6Ti_{2.6}Fe_{1.72}Mn_{0.68}O_{18}$ | 88 | 12 | 0.115 | 0.254 | 49.22 | 58.45 |
| $Bi_6Ti_{2.5}Fe_{1.82}Mn_{0.68}O_{18}$ | 87 | 13 | 0.124 | 0.227 | 49.08 | 58.05 |
| $Bi_6Ti_{2.5}Fe_{1.77}Mn_{0.73}O_{18}$ | 82 | 18 | 0.123 | 0.270 | 49.11 | 58.09 |
| $Bi_6Ti_{2.4}Fe_{1.92}Mn_{0.68}O_{18}$ | 80 | 20 | 0.127 | 0.288 | 48.75 | 57.85 |
| $Bi_6Ti_{2.3}Fe_{1.95}Mn_{0.75}O_{18}$ | 70 | 30 | 0.136 | 0.270 | 48.55 | 57.50 |
| $Bi_6Ti_{2.3}Fe_{2.00}Mn_{0.70}O_{18}$ | 0 | 100 | ⋯ | 0.223 | ⋯ | 57.67 |

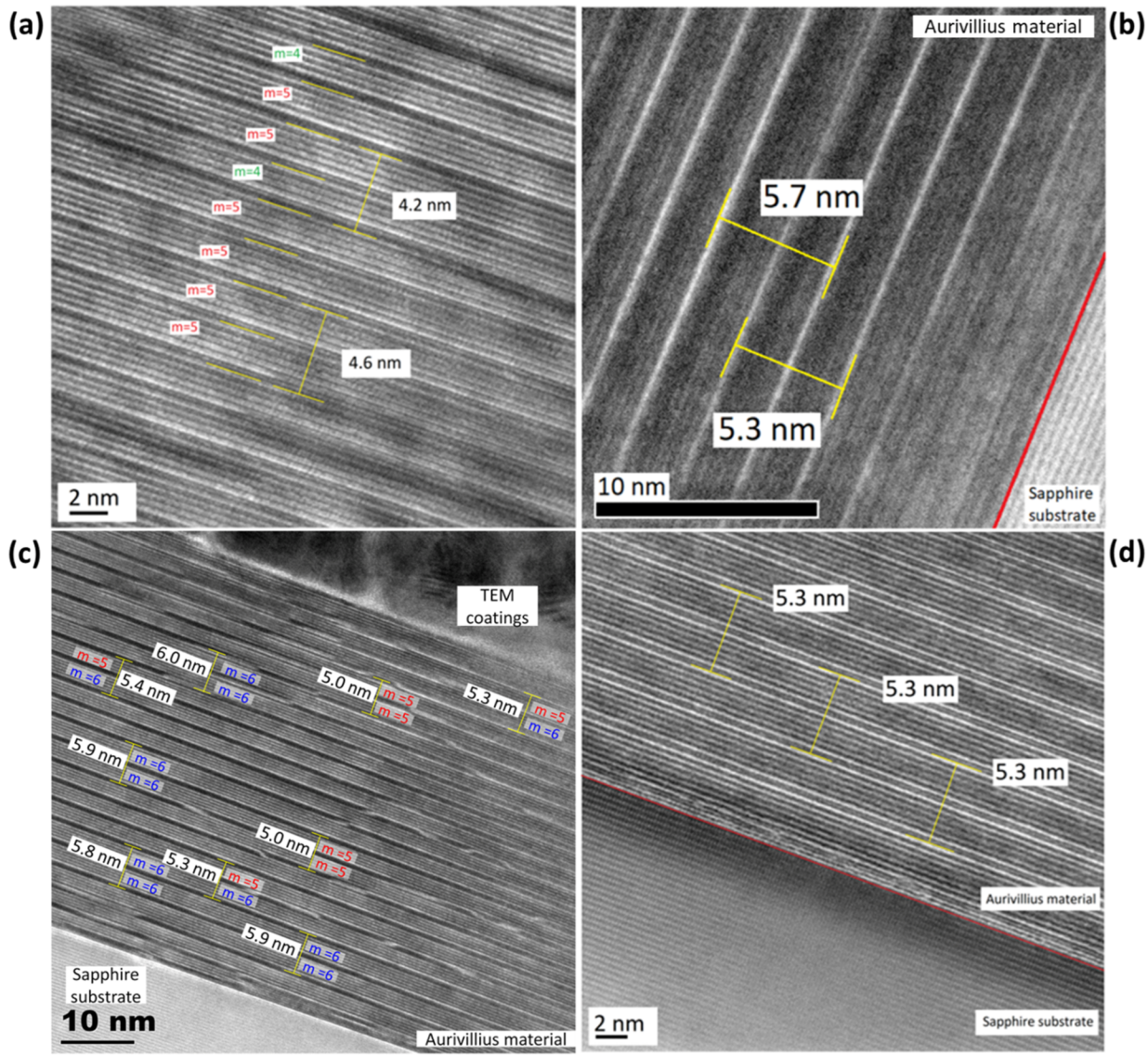



**FIG. 4.** TEM images of representative Aurivillius phase thin film samples from series 4: (a) and (b) $Bi_6Ti_{2.8}Fe_{1.52}Mn_{0.68}O_{18}$ and (c) and (d) $Bi_6Ti_{2.3}Fe_{1.95}Mn_{0.75}O_{18}$.

04 August 2025 15:15:43


© Author(s) 2025

$m$ = 6 phase ($c$-axis length of 5.9 ± 0.1 nm), accompanied by regions of the $m$ = 5 phases ($c$-axis length of 5.0 ± 0.1 nm).

TEM analysis also demonstrates the local structural complexity, highlighting stacking faults with sub-unit-cell intergrowths of various $m$-layers. In Fig. 4(a), TEM imaging shows small regions of the $m$ = 4 Aurivillius phase within the $Bi_6Ti_{2.8}Fe_{1.52}Mn_{0.68}O_{18}$ sample, where $m$ = 5 and $m$ = 4 intergrowths result in a $c$-axis length of 4.2 ± 0.1 nm (within 10% instrumental error of the expected average $c$-axis value of 4.5 nm). Figure 4(b) reveals local regions in the film with unit cell lengths matching the $m$ = 6 Aurivillius structure (5.7 ± 0.1 nm) and regions of $m$ = 6 structures intergrown with the $m$ = 5 phase (5.3 ± 0.1 nm). Similarly, Fig. 4(d) shows that for the $Bi_6Ti_{2.6}Fe_{1.72}Mn_{0.68}O_{18}$ composition, local areas exhibit unit cell lengths of 5.3 ± 0.1 nm, indicative of stacking fault intergrowths of $m$ = 5 (~4.9 nm) and $m$ = 6 (~5.7 nm) layers. These stacking fault intergrowths of different $m$ phases are frequently accompanied by OPB defects, which likely contribute to the peak broadening observed in the XRD patterns.

EDX compositional analysis confirmed the chemical composition of the films and the successful co-substitution of Mn and Fe into the $Bi_2O_2(Bi_{m-1}Ti_mO_{3m+1})$ Aurivillius phases (see Sec. SI6.3 of the supplementary material). While determining the oxidation states of Mn and Fe experimentally is important for elucidating the magnetic exchange interactions and mechanisms governing long-range magnetic order in these materials, previous STEM-EELS studies highlighted the challenges in accurately determining the Mn and Fe cation oxidation states.[25] These difficulties stem from the low signal-to-noise ratio in the Fe and Mn $L_{2,2}$-edges.

While an enhancement in magnetic moment is anticipated with higher magnetic cation content, a thorough analysis is essential to rule out contributions from trace magnetic impurities.[19,20,33,34] Establishing a defined confidence level for a material being single-phase, with magnetization being intrinsic to the Aurivillius phase, would require applying the methodology developed by Schmidt *et al.*[23] This procedure involves conducting measurements across varying sample volumes and instrument resolutions, followed by comprehensive full statistical analysis. However, such an in-depth analysis is outside the scope of the present article.

## B. Investigations of ferroelectric properties at the nanoscale as a function of composition and Aurivillius structure

Aurivillius phase materials are ferroelectrics in which the polarization is predominantly along the $a$-axis, in-plane direction.[12,17] Since these films are predominantly $c$-axis oriented, most grains have their crystallographic $a$-axis lying within the lateral plane of the film. However, due to the absence of an epitaxial relationship with the substrate and the isotropic random orientation of the plate-like crystals, ferroelectricity is not expected to exhibit anisotropy within the plane. We employed lateral piezoresponse force microscopy (PFM) to confirm in-plane piezoelectricity for samples with three different compositions: $Bi_6Ti_{2.80}Fe_{1.52}Mn_{0.68}O_{18}$ (56% Ti at the B-site), $Bi_6Ti_{2.50}Fe_{1.77}Mn_{0.73}O_{18}$ (50% Ti at the B-site), and $Bi_6Ti_{2.30}Fe_{1.95}Mn_{0.75}O_{18}$ (46% Ti at the B-site). The films are naturally self-polarized, and the amplitude of the piezoresponse in the lateral direction can be clearly observed in the single frequency (15 kHz) lateral PFM images in Fig. SI7 and lateral DART PFM images in Figs. 5(a) and 5(b). The regions of uniformly orientated polarity and piezoresponse are represented by polar domains, separated by domain walls. The experiments reveal an isotropic random distribution of in-plane domains, with no evidence of uniaxial in-plane ferroelectricity. Consistent with observations in other Aurivillius phases, the isotropic domain wall energy appears to govern domain morphology, resulting in irregularly shaped domains with curved walls.[59,60]

The substitution of Fe and Mn into the structure and the decrease in the Ti content does not seem to diminish the in-plane piezoresponse; a clear, lateral piezoresponse is demonstrated for all three compositions. This contrasts with the $m$ = 6 $Bi_7Mn_{3.75}Ti_{2.25}O_{21}$ Aurivillius phase composition reported by Zurbuchen *et al.*[22] for which 62.5% Mn at the B-site enabled ferromagnetic characteristics at 2 K, but this compromised the ferroelectric properties, to the extent that a reliable ferroelectric response could not be measured.

Aurivillius phases with $m$ = odd and $m$ = even exhibit different out-of-plane ferroelectric properties. Ferroelectric Aurivillius phases with $m$ = even (e.g., $m$ = 6) retain a mirror plane perpendicular to the $c$-axis. This prohibits out-of-plane polarization. Meanwhile, for ferroelectric Aurivillius phases with $m$ = odd (e.g., $m$ = 5), retention of the mirror plane is not energetically favorable, and a minor polarization is expected along the $c$-axis out-of-plane direction in conjunction with a major in-plane polarization.[61] It is thus expected that as the $m$ = 5 Aurivillius samples reorganize to accommodate more of the $m$ = 6 phase, the polarization response along the out-of-plane $c$-axis direction will decrease.

Vertical PFM studies were performed on representative samples to examine the local out-of-plane ferroelectric and piezoresponses as functions of composition and structure. Electromechanical switching properties were probed locally by vertical switching spectroscopy PFM (SS-PFM). The hysteresis loops' phase and amplitude as a function of applied electric field are shown in Figs. SI8, 5(c), and 5(d). The local polarization switching data reveal a 180° phase shift in the vertical direction across all three samples. However, the coercive field (calculated as the width of the hysteresis loop divided by the sample thickness) increases with higher magnetic cation content. In particular, it rises from 101.1 V/$\mu$m for $Bi_6Ti_{2.80}Fe_{1.52}Mn_{0.68}O_{18}$ [56% Ti at the B-site, Figs. 5(c) and 5(d)], to 338.2 V/$\mu$m for $Bi_6Ti_{2.50}Fe_{1.77}Mn_{0.73}O_{18}$ [50% Ti at the B-site, Figs. SI8(c) and SI8(d)], and further to 469.7 V/$\mu$m for $Bi_6Ti_{2.30}Fe_{1.95}Mn_{0.75}O_{18}$ [46% Ti at the B-site, Figs. SI8(e) and SI8(f)]. The vertical displacement amplitude as a function of the applied DC bias for the samples with 56% and 50% Ti at the B-site shows typical ferroelectric hysteresis loops, with piezoresponse values of 6.4 pm/V for $Bi_6Ti_{2.80}Fe_{1.52}Mn_{0.68}O_{18}$ [Fig. 5(c)] and 7.6 pm/V for $Bi_6Ti_{2.50}Fe_{1.77}Mn_{0.73}O_{18}$ [Fig. SI8(c)]. However, the vertical piezoresponse decreased to 3.6 pm/V for $Bi_6Ti_{2.30}Fe_{1.95}Mn_{0.75}O_{18}$ [50% Ti at the B-site, Fig. SI8(e)]. Furthermore, the hysteresis shape is not concave for the $Bi_6Ti_{2.30}Fe_{1.95}Mn_{0.75}O_{18}$ (46% Ti at the B-site) composition, resembling characteristics of a lossy dielectric.[62] For the Fe-containing $Bi_4Bi_{m-3}Fe_{m-3}Ti_3O_{3m+3}$ phases, it was previously shown that the leakage current increased as $m$ increased from 4 to 6.[63] The $Bi_6Ti_{2.30}Fe_{1.95}Mn_{0.75}O_{18}$ sample contains non-ferroelectric secondary-phase impurities, comprising a volume fraction of 2.7 vol. % (see SI6.3 of the supplementary material for details on the determination of this value). These impurities may contribute to

04 August 2025 15:15:43


© Author(s) 2025

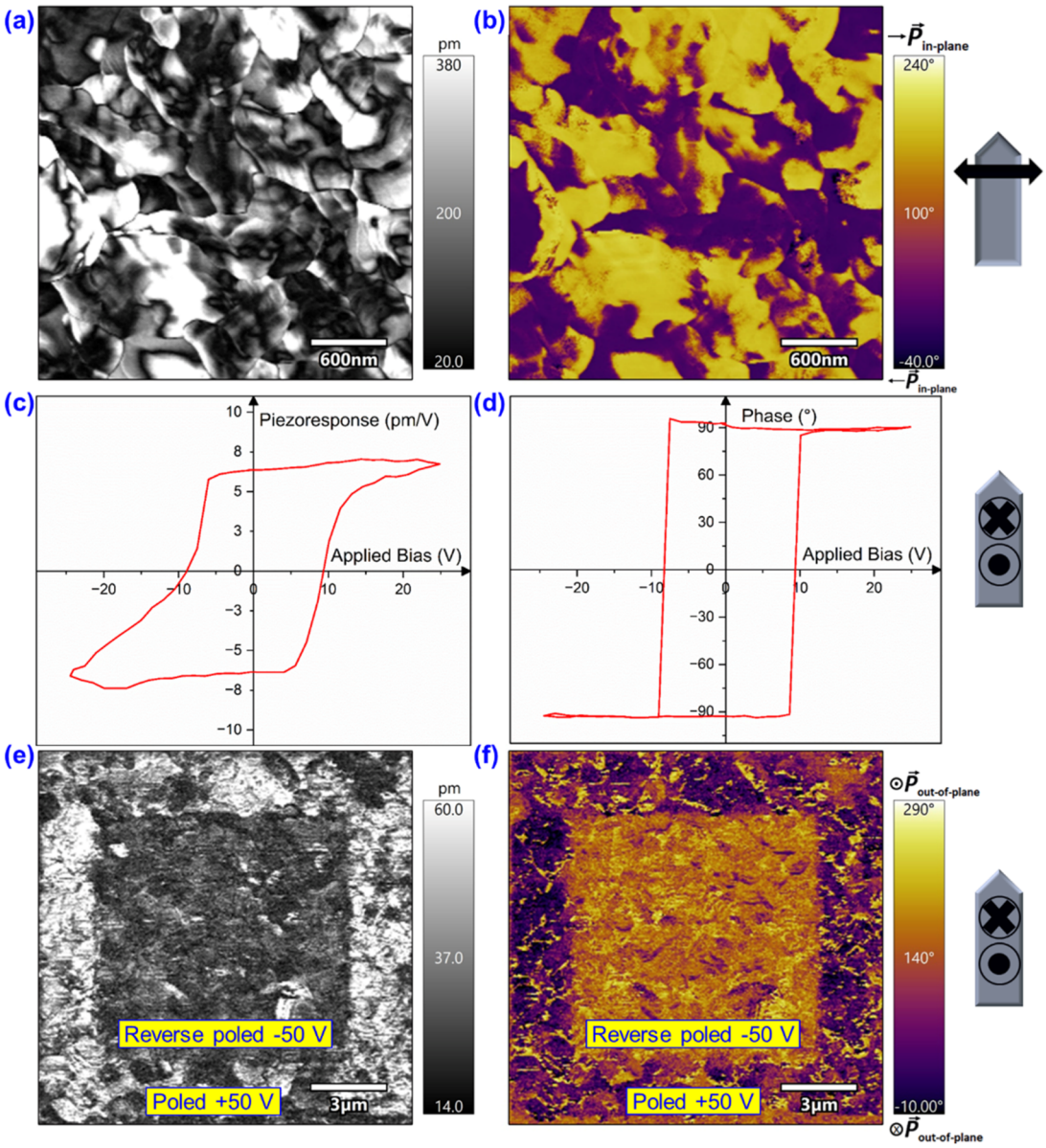



**FIG. 5.** (a) PFM amplitude and (b) PFM phase images from DART PFM measurements in the lateral direction for $Bi_6Ti_{2.30}Fe_{1.95}Mn_{0.75}O_{18}$ (46% Ti at the B-site). (c) and (d) Vertical DART-PFM switching spectroscopy: (c) piezoresponse and (d) phase loops on the removal of an applied DC bias (±25 V) for $Bi_6Ti_{2.80}Fe_{1.52}Mn_{0.68}O_{18}$ (56% Ti at the B-site). (e) and (f) Vertical PFM lithography data illustrating the reversibility of ferroelectric switching: (e) vertical PFM amplitude image and (f) vertical PFM phase image for $Bi_6Ti_{2.50}Fe_{1.77}Mn_{0.73}O_{18}$ (50% Ti at the B-site). Initially, a 15 × 15 $\mu m^2$ region was poled with a +50 V DC bias. Subsequently, a 10 × 10 $\mu m^2$ region within the poled area was reverse-poled using a −50 V DC bias.

domain wall pinning, the reduced polarization value, the increased coercive field, and an altered hysteresis loop shape. Furthermore, the presence of trace levels of secondary phase impurities would complicate attempts to measure a magnetic signal intrinsic to the main Aurivillius phase;[19,20,23,33,34,47] therefore, magnetic measurements of the new compositions could not be reliably performed in this work.

PFM bit-mapped voltage lithography (see SI2 of the supplementary material) enables the modification of the film's ferroelectric polarization by applying a bias voltage. When the applied electric field exceeds the local coercive field, it induces a reversal of the ferroelectric polarization. These investigations (Fig. SI9) confirm the trend that higher DC fields are required for vertical domain switching as the B-site Ti concentration

04 August 2025 15:15:43


© Author(s) 2025

decreases and the presence of the $m = 6$ phases increases. Applying a vertical DC bias of 50 V to specific regions on the thin film surface during the "write" step resulted in ferroelectric polarization reversal in both the $Bi_6Ti_{2.80}Fe_{1.52}Mn_{0.68}O_{18}$ (56% Ti at the B-site) and $Bi_6Ti_{2.50}Fe_{1.77}Mn_{0.73}O_{18}$ (50% Ti at the B-site) samples, as detected by the subsequent PFM scan during the "read" step [Figs. SI9(a)–SI9(d)]. However, in the $Bi_6Ti_{2.30}Fe_{1.95}Mn_{0.75}O_{18}$ (46% Ti at the B-site) sample, a higher DC bias of 90 V was necessary for vertical domain switching [Figs. SI9(e) and SI9(f)]. A closer examination of the vertical PFM lithography data (Fig. SI10) reveals successful ferroelectric switching on smoother film surfaces, as indicated by the formation of upward-oriented (yellow) domains. Conversely, switching proved more challenging on rougher surfaces, where some grains remained as downward-oriented (purple) domains. Figures 5(e), 5(f), SI11, and SI12 demonstrate the reversibility of vertical ferroelectric switching. Initially, specific regions of the films were poled using a positive DC bias. Subsequently, smaller areas within the positively poled regions were reverse-poled by applying an opposite, negative DC bias. The successful demonstration of reversibility indicates the ability to repeatedly write and erase ferroelectric domains with high spatial resolution, a critical requirement for advanced memory and logic devices.

## IV. DISCUSSION

### A. Structural adaptation of the Aurivillius system to higher *m* phases to compensate for charge and size variations during B-site substitution

Increasing the concentration of Mn and Fe in this work is motivated by the desire to increase the magnetic ion fraction (>40%) further beyond the percolation threshold[26] and to thereby enhance long-range magnetic ordering within the B6TFMO system. For a $Bi_6Ti_{2.3}Fe_{2.00}Mn_{0.70}O_{18}$ composition, the magnetic ion content would be 54% of B-site cations, which is 14% higher than the $Bi_6Ti_{2.99}Fe_{1.46}Mn_{0.55}O_{18}$ composition, which displays an $M_S$ value of 215 emu/cm$^3$.[20] However, the direct substitution of the lower valence $Mn^{3+}$ and $Fe^{3+}$ for $Ti^{4+}$ results in an unbalanced stoichiometry. Moreover, the substitution of $Ti^{4+}$ (0.605 Å) by $Fe^{3+}$ (0.645 Å) and $Mn^{3+}$ (0.645 Å) also involves accommodation of larger ionic radii, which could lead to distortion of the crystal structure. It is clear from the XRD and TEM analyses in this work that below a threshold of nominal 54% $Ti^{4+}$ (46% magnetic cations), the $m = 5$ structure rearranges into a mixed-phase material based on $m = 5$ and six-layered ($m = 6$) intergrowths and evolves into an $m = 6$ phase for the $Bi_6Ti_{2.3}Fe_{2.00}Mn_{0.70}O_{18}$ composition at 46% $Ti^{4+}$ (54% magnetic cations). In Sec. SI6 of the supplementary material, we explore the potential for alternative mechanisms that could compensate for charge and size differences when incorporating increased magnetic ion content within the B6TFMO Aurivillius phase system. From the argument in Sec. SI6.2 of the supplementary material, we infer that the decrease in $Ti^{4+}$ might be compensated in some part by the oxidation of $Mn^{3+}$ to $Mn^{4+}$. However, previous work on the Aurivillius phase structures demonstrated the difficulty in forming phase pure structures with substantial amounts of $Mn^{4+}$ on the B-site. For example, McCabe and Greaves[30] reported unsuccessful attempts to prepare $Bi_2Sr_2Nb_2MnO_{12}$ due to the inability to support a significant $Mn^{4+}$ content. Armstrong and Newnham observed that "*substantial substitution*" of B-site metals "*is obtained for only a narrow size range of octahedral ions*": 0.58 Å to 0.65 Å.[64] It is therefore expected that there will be a limit to how much $Mn^{4+}$ (octahedral site ionic radius 0.53 Å) can be accepted in the $m = 5$ B6TFMO structure. While the precipitation of trace levels (2.7 vol. %) of secondary phases has been observed for the $Bi_6Ti_{2.3}Fe_{1.95}Mn_{0.75}O_{18}$ composition and may assist with compensating some charge/size effects (see Sec. SI6.3 of the supplementary material), overall, XRD analysis (Fig. 2) and TEM imaging (Fig. 4) clearly demonstrate that the $m = 5$ Aurivillius structure adapts to a higher $m = 6$ layered homolog to accommodate increased levels (>46%) of magnetic cations.

Given that bismuth is used in excess during the synthesis, structural and compositional rearrangement from an $m = 5$ phase to an $m = 6$ phase is permitted based on the concentrations of cations available. To correlate the charge balancing requirements with the compositions where structural adaptation occurs, we tabulate the nominal B-site proportion of Ti, Fe, and Mn for the B6TFMO samples from a spread of compositions with decreasing Ti concentration in Table SI3 of the supplementary material. Next, we assume that Ti has a +4 valence and Fe has a +3 valence, and we let Mn have a valence of either +3 or +4. We then assume that the proportion of $Mn^{4+}$ present is proportional to the concentration necessary to maintain a charge balanced $m = 5$ Aurivillius structure (see SI7 of the supplementary material). Note that the displayed oxidation states are theoretical values based on nominal, assumed phase-pure compositions and are not taken from experimental measurements. The table is arranged in order of decreasing Ti concentration, and we correlate the compositions with the observations (from XRD and TEM data) of whether the sample shows an overall $m = 5$, $m = 6$, or mixed $m = 5/6$ Aurivillius phase. Table SI3 of the supplementary material follows the same trend as Table I and summarizes that the appearance of the $m = 6$ phase (as observed in the XRD and TEM analyses) follows a systematic trend with decreasing Ti concentration. More precisely, the structural rearrangement occurs when the combined concentration of Fe and Mn at the B-site of the perovskite units is above 46% (see Table SI3 of the supplementary material). Furthermore, when the nominal concentration of $Mn^{4+}$ is greater than 6.6%, meaning that the theoretical average oxidation state of Mn in the $m = 5$ structure is larger than ≈3.4, the appearance of the $m = 6$ phase begins to occur. It appears that the cation radius disparity restricts the maximum concentration of $Mn^{4+}$ that can be accommodated by the $m = 5$ structure, with a threshold $Mn^{4+}$ solubility limit of between 6.6% and 8.0% (or 46%–48% magnetic ion content at the B-site). We note that this is a similar average oxidation state threshold to that previously observed in other Aurivillius phase systems by Zurbuchen *et al.*[22] ($Mn^{3.2+}$) and McCabe and Greaves[30] ($Mn^{3.4+}$).

With direct evidence from TEM and XRD analyses showing the evolution of the $m = 6$ phase as the concentration of Ti decreases and the levels of Fe and Mn increase, we next explore how the structural rearrangement of the Aurivillius phase to higher $m$ values accommodates the increased Mn content. Theoretical scenarios are outlined in Table II. For example, consider the chemical composition of the $m = 5$ $Bi_6Ti_{2.30}Fe_{2.00}Mn_{0.70}O_{18}$ phase. When rearranged into the $m = 6$ structure, it assumes the composition $Bi_7Ti_{2.76}Fe_{2.40}Mn_{0.84}O_{21}$. In Table II, for the $m = 5$ phase (composition $Bi_6Ti_{2.30}Fe_{2.00}Mn_{0.70}O_{18}$), the average oxidation state of Mn is calculated to be +4.00, assuming

04 August 2025 15:15:43


© Author(s) 2025

**TABLE II.** Examples of stoichiometry/oxidation state calculations for $m = 5$ and $m = 6$ Aurivillius phases.

| Composition | Ti(IV) B-site (%) | Fe(III) B-site (%) | Mn B-site (%) | Mn(IV)% of Mn | Mn(IV)% overall | Mn o.s. | Tolerance factor |
|---|---|---|---|---|---|---|---|
| $Bi_6Ti_{2.30}Fe_{2.00}Mn_{0.70}O_{18}$ $m = 5$ | 46 | 40 | 14 | 100 | 14.00 | +4.00 | 0.85 |
| $Bi_7Ti_{2.76}Fe_{2.40}Mn_{0.84}O_{21}$ $m = 6$ | 46 | 40 | 14 | 29 | 4.06 | +3.29 | 0.87 |
| $Bi_6Ti_{2.30}Fe_{1.95}Mn_{0.75}O_{18}$ $m = 5$ | 46 | 39 | 15 | 93 | 13.95 | +3.93 | 0.85 |
| $Bi_7Ti_{2.76}Fe_{2.34}Mn_{0.90}O_{21}$ $m = 6$ | 46 | 39 | 15 | 26 | 3.90 | +3.27 | 0.87 |

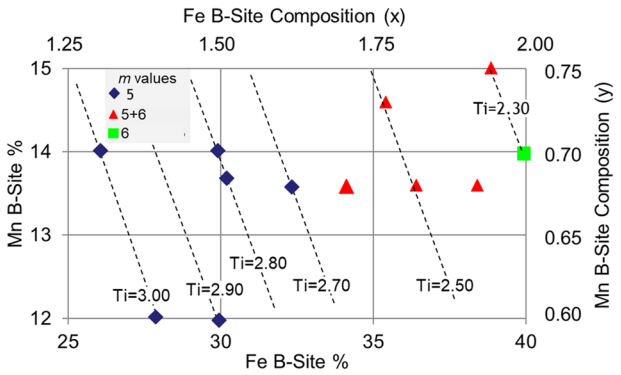



**FIG. 6.** Composition map demonstrating the $m$ number for a spread of B6TFMO compositions where the Mn concentration is varied from 0.60 to 0.75.

oxidation states of +4 for Ti and +3 for Fe. When the same ratio of Ti, Fe, and Mn cations is applied to the $m = 6$ structure (composition $Bi_7Ti_{2.76}Fe_{2.40}Mn_{0.84}O_{21}$), the average oxidation state of Mn is calculated to be +3.29. The value falls within the range reported for stable Aurivillius phase compositions by Zurbuchen *et al.*[22] ($Mn^{3.2+}$) and McCabe and Greaves[30] ($Mn^{3.4+}$). It is important to note that while the relative proportions of the B-site atoms remain the same for both arrangements (as shown in Table II), the proportion of $Mn^{4+}$ required to achieve charge-balanced stoichiometry is significantly lower for the $m = 6$ phase (4.06% $Mn^{4+}$) compared to the $m = 5$ phase (14.00% $Mn^{4+}$). This explains how the formation of the higher $m = 6$ Aurivillius phase allows for the accommodation of a higher concentration of magnetic cations while maintaining balanced stoichiometry.

We propose that the inability of the $m = 5$ Aurivillius structure to accommodate $Mn^{4+}$ concentrations above 6.6% at the B-site likely drives the structural rearrangement observed, leading to the formation of a higher $m$-phase, as evidenced by XRD and TEM analyses. This rearrangement, along with an increased number of A-site cations, is posited to enhance the tolerance factor of the perovskite unit (see Sec. SI8 of the supplementary material), as shown in Table II. The structural adaptation to incorporate higher magnetic cation content in the B6TFMO Aurivillius phases is summarized in the composition map in Fig. 6, where the Mn concentration varies from 0.60 to 0.75, complementing the modeled XRD data in Table I.

This observation of structural reorganization into a higher-layered $m = 6$ Aurivillius phase to accommodate increased magnetic fraction is particularly interesting. At large values of $m$, the free energy of formation in Aurivillius phases becomes thermodynamically degenerate, making the synthesis of higher layered ($m > 5$) homologs challenging. These phases are typically difficult to achieve without the support of epitaxial substrates or kinetically controlled growth conditions.[22,56,65] This work progresses previous studies by Sun *et al.*[52,66] on nanoscale layer-stacking evolutions of disordered $m = 4$ and $m = 5$ phases and Deepak *et al.*[53] of tunable structural changes from an $m = 3$ phase ($Bi_4Ti_3O_{12}$) to an $m = 4$ phase ($Bi_5Ti_3FeO_{15}$) on the addition of Fe precursor during chemical vapor deposition growth. The preceding studies of Deepak *et al.*[53] revealed that the only way to accommodate an increase in Fe and to maintain charge balance between differently charged $Fe^{3+}$ and $Ti^{4+}$ was to accommodate regions of the four-layered Aurivillius structure, accompanied by OPB defects. As the Fe concentration was increased further, there was an increase in the random stacking of $m = 4$ layers between $m = 3$ layers and an increase in $c$-axis lattice parameter from 32.274 to 40.727 Å. Work by Deepak *et al.*[53] and the current work are examples of charge mediated synthesis, which involves the exploitation of constituents having similar coordination chemistry but different layer charges to impose a particular layer order during crystallization of a thin film and yield large electronically neutral structural units. In the absence of bulk thermodynamic stability, utilization of the layer-to-layer charge disparities between the $[Bi_2O_2]^{2+}$ fluorite layers and atomic layers within the perovskite blocks has been shown to stabilize Aurivillius phase homologs with larger values of $m$ (e.g., $m = 7$ $Sr_4Bi_4Ti_7O_{24}$),[56] in contrast to Ruddlesden–Popper phases, which possess charge-neutral layers. The $m = 7$ $Sr_4Bi_4Ti_7O_{24}$ phases were synthesized in the kinetic limit using pulsed laser deposition on epitaxial [$SrTiO_3$ (001)], $LaAlO_3$ $(001)_c$, and $SrRuO_3$ $(001)_c/SrTiO_3$ (001) substrates.[56] Alternatively, the work presented in this contribution demonstrates that using transition metal cations for aliovalent substitution in straightforward chemical solution deposition processes can overcome thermodynamic challenges in synthesizing higher-layered Aurivillius homologs. This approach has eliminated the need for epitaxial substrates or kinetically limited growth processes for this Bi/Ti/Mn/Fe-based material system.

## V. CONCLUSIONS

Research highlights that a key requirement for technologically viable multiferroics, suitable for ultralow-power memory devices, is the enhancement of remanent magnetic moment at room temperature.[4] To meet this demand, this study investigates the effect of

04 August 2025 15:15:43


© Author(s) 2025

increased magnetic ion substitution on the crystal structure of multiferroic Aurivillius phases, driven by the expectation that increased magnetic ion content will improve magnetization. It provides a comprehensive understanding of the structural adaptations that occur to accommodate charge and size disparities associated with higher concentrations of magnetic cations in these materials. The initial investigation focused on determining the solubility limit for magnetic Fe and Mn cations within the $m = 5$ Aurivillius phase structure. The XRD and TEM analyses of $Bi_6Ti_xFe_yMn_zO_{18}$ (x = 2.3–3.2, y = 1.2–2.0, z = 0.3–0.9) compositions revealed that when the $Ti^{4+}$ content was lowered below 54%, a discernible transformation occurs, leading to the formation of a mixed-phase sample consisting of both the main $m = 5$ Aurivillius phase and the $m = 6$ phase. The prevalence of the $m = 6$ phase within the $m = 5$ phase matrix increased with decreasing $Ti^{4+}$ content. Upon elevating the nominal $Mn^{4+}$ content to 14%, the $m = 5$ structure transforms into a single-phase $m = 6$ structure, with each perovskite block now containing nominal 4% $Mn^{4+}$. The transition to the higher-layered Aurivillius homolog is interesting, especially considering the thermodynamic constraints on expanding layering periods.[56] It suggests that chemical modifications are pivotal in stabilizing the formation of the $m = 6$ Aurivillius phase. Furthermore, this study demonstrates how aliovalent substitution can overcome these thermodynamic challenges, enabling the synthesis of higher-layered Aurivillius homologs without relying on epitaxial growth or kinetically constrained methods.

This transition to the higher $m = 6$ phase reduces the relative fraction of $Mn^{4+}$ required for charge neutrality in the material (refer to Table II). Consequently, the structure becomes more tolerant of higher magnetic cation content. Correspondingly, the average calculated oxidation state for Mn also decreases, falling within the range of values reported previously[22,30] for stable Aurivillius phase compositions. Moreover, the percolation fraction, which is crucial for long-range magnetic ordering, also increases upon phase transformation. For instance, in the $m = 6$ composition $Bi_7Ti_{2.76}Fe_{2.34}Mn_{0.90}O_{21}$, the magnetic cation content reaches 54% of B-site cations, which is 14% higher than the $m = 5$ multiferroic $Bi_6Ti_{2.99}Fe_{1.46}Mn_{0.55}O_{18}$ composition that exhibits an $M_S$ value of 215 emu/cm$^3$.[20] Increasing the magnetic cation content is envisaged to enhance the magnetic moment and multiferroic properties of the new Aurivillius phase compositions. However, a thorough phase purity analysis will be necessary before reliable magnetometry studies can be performed in future work. As expected from crystal symmetry, the minor out-of-plane ferroelectric response diminishes with increasing structural reorganization toward the $m = 6$ phase. Notably, the predominant in-plane piezoresponse of these materials is unaffected by magnetic cation substitution.

This study provides valuable insights into the limiting factors that govern magnetic ion substitution at the B-site of Aurivillius materials, which should be considered during the development of new multiferroic materials. Although the films prepared in this study were ~90 nm thick with an rms roughness value of ~20 nm, making them unsuitable for immediate device integration, our previous work with chemical vapor deposition (CVD) successfully demonstrated the growth of 5 nm $m = 5$ Aurivillius phase films with an rms roughness of ~1 nm.[45] Future work employing CVD and charge-mediated synthesis, which has proven effective for growing epitaxial thin films of higher-layered homologs,[56] offers a feasible path toward achieving thinner $m = 6$ films with comparable properties. This study, focusing on incorporating higher magnetic cation content, highlights the potential for enhancing magnetic properties in room-temperature multiferroic materials, laying the foundation for the development of technologically viable ultralow-power memory devices.

## SUPPLEMENTARY MATERIAL

See the supplementary material for details on contributions to long-range magnetic order in Aurivillius phase systems, supplementary methods, supplementary XRD and PFM data, the calculation of full width half maxima (FWHM) values for Aurivillius phases with decreased Ti concentrations, possible alternate charge/size compensation mechanisms, the approximation of the Mn oxidation state, and the calculation of the tolerance factor. Further information on the x-ray diffraction (XRD) pattern simulations of $m = 5$, $m = 6$, and mixed $m = 5/m = 6$ Aurivillius phase structures is included to support this study.

## ACKNOWLEDGMENTS

The authors acknowledge the support of Science Foundation Ireland (SFI) Principle Investigator Award No. 15/IA/3015 DEPOMan, "Design, Deposition and Exploitation of Novel Micro and Nano-scale Materials and Devices for Advanced Manufacturing," support of SFI under the FORME Strategic Research Cluster Award No. 07/SRC/I1172, support from the SFI Frontiers for the Future Project No. 19/FFP/6475, and support from the Royal Society and SFI University Fellowships Nos. UF 140263 and URF\R\201008. J.H. and L.K. thank Professor Martyn Pemble (Emeritus, University College Cork) for his mentorship during this project.

## AUTHOR DECLARATIONS

### Conflict of Interest

The authors have no conflicts to disclose.

### Author Contributions

**Jennifer Halpin**: Data curation (equal); Formal analysis (equal); Investigation (equal); Methodology (equal); Validation (equal); Visualization (equal); Writing – original draft (equal); Writing – review & editing (equal). **Michael Schmidt**: Data curation (equal); Formal analysis (equal); Investigation (equal); Validation (equal); Visualization (equal); Writing – review & editing (supporting). **Roger W. Whatmore**: Conceptualization (equal); Formal analysis (equal); Investigation (equal); Methodology (equal); Supervision (equal); Validation (equal); Visualization (equal); Writing – original draft (equal); Writing – review & editing (equal). **Lynette Keeney**: Conceptualization (lead); Data curation (equal); Formal analysis (equal); Funding acquisition (lead); Investigation (equal); Methodology (equal); Project administration (lead); Resources (lead); Supervision (equal); Validation (equal); Visualization (equal); Writing – original draft (equal); Writing – review & editing (equal).

04 August 2025 15:15:43


© Author(s) 2025

## DATA AVAILABILITY

The data that support the findings of this study are available within the article and its supplementary material.

## REFERENCES


[1] K. Bartley, Big statistics: How much data is there in the world?, https://rivery.io/blog/big-data-statistics-how-much-data-is-there-in-the-world/.

[2] E. Masanet, A. Shehabi, N. Lei, S. Smith, and J. Koomey, "Recalibrating global data center energy-use estimates," Science **367**(6481), 984–986 (2020).

[3] S. Manipatruni, D. E. Nikonov, and I. A. Young, "Beyond CMOS computing with spin and polarization," Nat. Phys. **14**(4), 338–343 (2018).

[4] N. A. Spaldin and R. Ramesh, "Advances in magnetoelectric multiferroics," Nat. Mater. **18**(3), 203–212 (2019).

[5] M. Buzzi, R. V. Chopdekar, J. L. Hockel, A. Bur, T. Wu, N. Pilet, P. Warnicke, G. P. Carman, L. J. Heyderman, and F. Nolting, "Single domain spin manipulation by electric fields in strain coupled artificial multiferroic nanostructures," Phys. Rev. Lett. **111**(2), 027204 (2013).

[6] C. A. Fernandes Vaz and U. Staub, "Artificial multiferroic heterostructures," J. Mater. Chem. C **1**(41), 6731–6742 (2013).

[7] E. Gradauskaite, Q. N. Meier, N. Gray, M. F. Sarott, T. Scharsach, M. Campanini, T. Moran, A. Vogel, K. Del Cid-Ledezma, B. D. Huey, M. D. Rossell, M. Fiebig, and M. Trassin, "Defeating depolarizing fields with artificial flux closure in ultrathin ferroelectrics," Nat. Mater. **22**(12), 1492–1498 (2023).

[8] F. Yang, M. H. Tang, Z. Ye, Y. C. Zhou, X. J. Zheng, J. X. Tang, J. J. Zhang, and J. He, "Eight logic states of tunneling magnetoelectroresistance in multiferroic tunnel junctions," J. Appl. Phys. **102**(4), 044504 (2007).

[9] E. C. Subbarao, "Ferroelectricity in $Bi_4Ti_3O_{12}$ and its solid solutions," Phys. Rev. **122**(3), 804–807 (1961).

[10] B. Aurivilllius, "Mixed bismuth oxides with layer lattices I. The structure type of $CaNb_2Bi_2O_9$," Ark. Kemi **1**(54), 463–480 (1949).

[11] B. Aurivillius, "Mixed bismuth oxides with layer lattices. 2. Structure of $Bi_4Ti_3O_{12}$," Ark. Kemi **1**(58), 499–512 (1949).

[12] L. Keeney, L. Colfer, D. Dutta, M. Schmidt, and G. Wei, "What lies beneath? Investigations of atomic force microscopy-based nano-machining to reveal subsurface ferroelectric domain configurations in ultrathin films," Microstructures **3**(4), 2023041 (2023).

[13] E. Gradauskaite, M. Campanini, B. Biswas, C. W. Schneider, M. Fiebig, M. D. Rossell, and M. Trassin, "Robust in-plane ferroelectricity in ultrathin epitaxial Aurivillius films," Adv. Mater. Interfaces **7**(14), 2000202 (2020).

[14] L. Keeney, R. J. Smith, M. Palizdar, M. Schmidt, A. J. Bell, J. N. Coleman, and R. W. Whatmore, "Ferroelectric behavior in exfoliated 2D Aurivillius oxide flakes of sub-unit cell thickness," Adv. Electron. Mater. **6**(3), 1901264 (2020).

[15] E. Gradauskaite, N. Gray, M. Campanini, M. D. Rossell, and M. Trassin, "Nanoscale design of high-quality epitaxial Aurivillius thin films," Chem. Mater. **33**(23), 9439–9446 (2021).

[16] S. Tinte and M. G. Stachiotti, "Multiferroic behavior of Aurivillius $Bi_4Mn_3O_{12}$ from first principles," Phys. Rev. B **85**(22), 224112 (2012).

[17] R. E. Newnham, R. W. Wolfe, and J. F. Dorrian, "Structural basis of ferroelectricity in the bismuth titanate family," Mater. Res. Bull. **6**(10), 1029–1039 (1971).

[18] A. T. Giddings, M. C. Stennett, D. P. Reid, E. E. McCabe, C. Greaves, and N. C. Hyatt, "Synthesis, structure and characterisation of the $n = 4$ Aurivillius phase $Bi_5Ti_3CrO_{15}$," J. Solid State Chem. **184**(2), 252–263 (2011).

[19] L. Keeney, T. Maity, M. Schmidt, A. Amann, N. Deepak, N. Petkov, S. Roy, M. E. Pemble, and R. W. Whatmore, "Magnetic field-induced ferroelectric switching in multiferroic Aurivillius phase thin films at room temperature," J. Am. Ceram. Soc. **96**(8), 2339–2357 (2013).

[20] A. Faraz, T. Maity, M. Schmidt, N. Deepak, S. Roy, M. E. Pemble, R. W. Whatmore, and L. Keeney, "Direct visualization of magnetic-field-induced magnetoelectric switching in multiferroic Aurivillius phase thin films," J. Am. Ceram. Soc. **100**(3), 975–987 (2017).

[21] L. Keeney, C. Downing, M. Schmidt, M. E. Pemble, V. Nicolosi, and R. W. Whatmore, "Direct atomic scale determination of magnetic ion partition in a room temperature multiferroic material," Sci. Rep. **7**(1), 1737 (2017).

[22] M. A. Zurbuchen, R. S. Freitas, M. J. Wilson, P. Schiffer, M. Roeckerath, J. Schubert, M. D. Biegalski, G. H. Mehta, D. J. Comstock, J. H. Lee, Y. Jia, and D. G. Schlom, "Synthesis and characterization of an $n = 6$ Aurivillius phase incorporating magnetically active manganese, $Bi_{7(}Mn, Ti)_6O_{21}$," Appl. Phys. Lett. **91**(3), 033113 (2007).

[23] M. Schmidt, A. Amann, L. Keeney, M. E. Pemble, J. D. Holmes, N. Petkov, and R. W. Whatmore, "Absence of evidence ≠ evidence of absence: Statistical analysis of inclusions in multiferroic thin films," Sci. Rep. **4**(1), 5712 (2014).

[24] K. Moore, E. N. O'Connell, S. M. Griffin, C. Downing, L. Colfer, M. Schmidt, V. Nicolosi, U. Bangert, L. Keeney, and M. Conroy, "Charged domain wall and polar vortex topologies in a room-temperature magnetoelectric multiferroic thin film," ACS Appl. Mater. Interfaces **14**(4), 5525–5536 (2022).

[25] L. Colfer, N. Bagués, M. Noor-A-Alam, M. Schmidt, M. Nolan, D. W. McComb, and L. Keeney, "Tilting and distortion in the multiferroic Aurivillius phase $Bi_6Ti_3Fe_{1.5}Mn_{0.5}O_{18}$," Chem. Mater. **36**, 5474 (2024).

[26] Ł. Kurzawski and K. Malarz, "Simple cubic random-site percolation thresholds for complex neighbourhoods," Rep. Math. Phys. **70**(2), 163–169 (2012).

[27] A. Y. L. Birenbaum-Haligua, "Can the Aurivillius phases be multiferroic? A first principles based study," Doctoral Thesis (ETH Zurich, 2015).

[28] R. D. Shannon, "Revised effective ionic radii and systematic studies of interatomic distances in halides and chalcogenides," Acta Crystallogr., Sect. A **32**(5), 751–767 (1976).

[29] H. Sun, Y. Wu, X. Xie, Y. Lu, T. Yao, J. Zhong, and X. Chen, "Ferroelectric, magnetic, and optical properties of Aurivillius compound $Bi_5FeTi_{2.5}Co_{0.5}O_{15}$," J. Materiomics **4**(4), 353–359 (2018).

[30] E. E. McCabe and C. Greaves, "Structural and magnetic characterisation of $Bi_2Sr_{1.4}La_{0.6}Nb_2MnO_{12}$ and its relationship to '$Bi_2Sr_2Nb_2MnO_{12}$,'" J. Mater. Chem. **15**(1), 177–182 (2005).

[31] T. Rojac, A. Bencan, G. Drazic, N. Sakamoto, H. Ursic, B. Jancar, G. Tavcar, M. Makarovic, J. Walker, B. Malic, and D. Damjanovic, "Domain-wall conduction in ferroelectric $BiFeO_3$ controlled by accumulation of charged defects," Nat. Mater. **16**(3), 322–327 (2017).

[32] A. Snedden, S. M. Blake, and P. Lightfoot, "Oxide ion conductivity in Ga-doped Aurivillius phases—A reappraisal," Solid State Ionics **156**(3), 439–445 (2003).

[33] L. Keeney, S. Kulkarni, N. Deepak, M. Schmidt, N. Petkov, P. F. Zhang, S. Cavill, S. Roy, M. E. Pemble, and R. W. Whatmore, "Room temperature ferroelectric and magnetic investigations and detailed phase analysis of Aurivillius phase $Bi_5Ti_3Fe_{0.7}Co_{0.3}O_{15}$ thin films," J. Appl. Phys. **112**(5), 052010 (2012).

[34] A. Faraz, J. Ricote, R. Jimenez, T. Maity, M. Schmidt, N. Deepak, S. Roy, M. E. Pemble, and L. Keeney, "Exploring ferroelectric and magnetic properties of Tb-substituted $m = 5$ layered Aurivillius phase thin films," J. Appl. Phys. **123**(12), 124101 (2018).

[35] E. Gradauskaite, K. A. Hunnestad, Q. N. Meier, D. Meier, and M. Trassin, "Ferroelectric domain engineering using structural defect ordering," Chem. Mater. **34**(14), 6468–6475 (2022).

[36] T. Patri, A. Ghosh, M. L. V. Mahesh, P. D. Babu, S. K. Mandal, and M. N. Singh, "Fortified relaxor ferroelectricity of rare earth substituted 4-layered $BaBi_{3.9}RE_{0.1}Ti_4O_{15}$ (RE = La, Pr, Nd, and Sm) Aurivillius compounds," Sci. Rep. **12**(1), 16508 (2022).

[37] F. Huang, X. Lu, T. Xu, Y. Liu, W. Su, Y. Jin, Y. Kan, and J. Zhu, "Multiferroic properties of Co and Nd Co-substituted $Bi_5Ti_3FeO_{15}$ thin films," Thin Solid Films **520**(21), 6489–6492 (2012).

[38] B. H. Park, B. S. Kang, S. D. Bu, T. W. Noh, J. Lee, and W. Jo, "Lanthanum-substituted bismuth titanate for use in non-volatile memories," Nature **401**(6754), 682–684 (1999).

[39] C. H. Hervoches, A. Snedden, R. Riggs, S. H. Kilcoyne, P. Manuel, and P. Lightfoot, "Structural behavior of the four-layer Aurivillius-phase ferroelectrics $SrBi_4Ti_4O_{15}$ and $Bi_5Ti_3FeO_{15}$," J. Solid State Chem. **164**(2), 280–291 (2002).

[40] M. García-Guaderrama, L. Fuentes-Montero, A. Rodriguez, and L. Fuentes, "Structural characterization of $Bi_6Ti_3Fe_2O_{18}$ obtained by molten salt synthesis," Integr. Ferroelectr. **83**(1), 41–47 (2006).


04 August 2025 15:15:43


© Author(s) 2025

[41]M. Krzhizhanovskaya, S. Filatov, V. Gusarov, P. Paufler, R. Bubnova, M. Morozov, and D. C. Meyer, "Aurivillius phases in the $Bi_4Ti_3O_{12}/BiFeO_3$ system: Thermal behaviour and crystal structure," Z. Anorg. Allg. Chem. **631**(9), 1603–1608 (2005).
[42]K. Momma and F. Izumi, "*VESTA 3* for three-dimensional visualization of crystal, volumetric and morphology data," J. Appl. Crystallogr. **44**(6), 1272–1276 (2011).
[43]J. B. Goodenough, "Jahn-Teller phenomena in solids," Annu. Rev. Mater. Res. **28**(1), 1–27 (1998).
[44]M. A. Zurbuchen, W. Tian, X. Q. Pan, D. Fong, S. K. Streiffer, M. E. Hawley, J. Lettieri, Y. Jia, G. Asayama, S. J. Fulk, D. J. Comstock, S. Knapp, A. H. Carim, and D. G. Schlom, "Morphology, structure, and nucleation of out-of-phase boundaries (OPBs) in epitaxial films of layered oxides," J. Mater. Res. **22**(6), 1439–1471 (2007).
[45]L. Keeney, Z. Saghi, M. O'Sullivan, J. Alaria, M. Schmidt, and L. Colfer, "Persistence of ferroelectricity close to unit-cell thickness in structurally disordered Aurivillius phases," Chem. Mater. **32**(24), 10511–10523 (2020).
[46]L. Keeney, L. Colfer, and M. Schmidt, "Probing ferroelectric behavior in sub-10 nm bismuth-rich Aurivillius films by piezoresponse force microscopy," Microsc. Microanal. **28**(4), 1396–1406 (2022).
[47]M. Palizdar, T. P. Comyn, M. B. Ward, A. P. Brown, J. P. Harrington, S. Kulkarni, L. Keeney, S. Roy, M. Pemble, R. Whatmore, C. Quinn, S. H. Kilcoyne, and A. J. Bell, "Crystallographic and magnetic identification of secondary phase in orientated $Bi_5Fe_{0.5}Co_{0.5}Ti_3O_{15}$ ceramics," J. Appl. Phys. **112**(7), 073919 (2012).
[48]Zulhadjri, T. P. Wendari, M. Ikhram, Y. E. Putri, U. Septiani, and Imelda, "Enhanced dielectric and ferroelectric responses in $La^{3+}/Ti^{4+}$ Co-substituted $SrBi_2Ta_2O_9$ Aurivillius phase," Ceram. Int. **48**(7), 10328–10332 (2022).
[49]Y. Li, M. Bian, N. Zhang, W. Bai, J. Yang, Y. Zhang, X. Tang, and J. Chu, "Mn-doping composition dependence of the structures, electrical and magnetic properties, and domain structure/switching of Aurivillius $Bi_5Ti_3FeO_{15}$ films," Ceram. Int. **45**(7), 8634–8639 (2019).
[50]A. Sanson and R. W. Whatmore, "Phase diagram of the $Bi_4Ti_3O_{12}$–$BaTiO_3$–$(Na_{1/2}Bi_{1/2})TiO_3$ system," J. Am. Ceram. Soc. **88**(11), 3147–3153 (2005).
[51]C. F. Holder and R. E. Schaak, "Tutorial on powder X-ray diffraction for characterizing nanoscale materials," ACS Nano **13**(7), 7359–7365 (2019).
[52]S. Sun, J. Shen, D. Yang, W. Han, R. Ti, and X. Yin, "Strong magnetic response regulated by layer-stacking perturbations in an Aurivillius-phase oxide," Mater. Lett. **357**, 135720 (2024).
[53]N. Deepak, P. Carolan, L. Keeney, M. E. Pemble, and R. W. Whatmore, "Tunable nanoscale structural disorder in Aurivillius phase, $n = 3$ $Bi_4Ti_3O_{12}$ thin films and their role in the transformation to $n = 4$, $Bi_5Ti_3FeO_{15}$ phase," J. Mater. Chem. C **3**(22), 5727–5732 (2015).
[54]N. Deepak, P. F. Zhang, L. Keeney, M. E. Pemble, and R. W. Whatmore, "Atomic vapor deposition of bismuth titanate thin films," J. Appl. Phys. **113**(18), 187207 (2013).
[55]T. Ungár, "Microstructural parameters from X-ray diffraction peak broadening," Scr. Mater. **51**(8), 777–781 (2004).
[56]M. A. Zurbuchen, V. O. Sherman, A. K. Tagantsev, J. Schubert, M. E. Hawley, D. D. Fong, S. K. Streiffer, Y. Jia, W. Tian, and D. G. Schlom, "Synthesis, structure, and electrical behavior of $Sr_4Bi_4Ti_7O_{24}$," J. Appl. Phys. **107**(2), 024106 (2010).
[57]N. A. Lomanova, M. I. Morozov, V. L. Ugolkov, and V. V. Gusarov, "Properties of Aurivillius phases in the $Bi_4Ti_3O_{12}$-$BiFeO_3$ system," Inorg. Mater. **42**(2), 189–195 (2006).
[58]Ismunandar, T. Kamiyama, A. Hoshikawa, Q. Zhou, B. J. Kennedy, Y. Kubota, and K. Kato, "Structural studies of five layer Aurivillius oxides: $A_2Bi_4Ti_5O_{18}$ (A = Ca, Sr, Ba and Pb)," J. Solid State Chem. **177**(11), 4188–4196 (2004).
[59]Y. L. Li, L. Q. Chen, G. Asayama, D. G. Schlom, M. A. Zurbuchen, and S. K. Streiffer, "Ferroelectric domain structures in $SrBi_2Nb_2O_9$ epitaxial thin films: Electron microscopy and phase-field simulations," J. Appl. Phys. **95**(11), 6332–6340 (2004).
[60]M. A. Zurbuchen, G. Asayama, D. G. Schlom, and S. K. Streiffer, "Ferroelectric domain structure of $SrBi_2Nb_2O_9$ epitaxial thin films," Phys. Rev. Lett. **88**(10), 107601 (2002).
[61]S. Trolier-McKinstry, "Crystal chemistry of piezoelectric materials," in *Piezoelectric and Acoustic Materials for Transducer Applications*, edited by A. Safari and E. K. Akdoğan (Springer, Boston, MA, 2008), pp. 39–56.
[62]J. F. Scott, "Ferroelectrics go bananas," J. Phys.: Condens. Matter **20**(2), 021001 (2007).
[63]D. Song, J. Yang, B. Yang, L. Chen, F. Wang, and X. Zhu, "Evolution of structure and ferroelectricity in Aurivillius $Bi_4Bi_{n-3}Fe_{n-3}Ti_3O_{3n+3}$ thin films," J. Mater. Chem. C **6**(32), 8618–8627 (2018).
[64]R. A. Armstrong and R. E. Newnham, "Bismuth titanate solid solutions," Mater. Res. Bull. **7**(10), 1025–1034 (1972).
[65]L. Eyring and M. O'Keeffe, "Chemistry of extended defects in non-metallic solids," in Proceedings of the Institute for Advanced Study, Scottsdale, AZ, 16–26 April 1969; 1970.
[66]S. Sun, Y. Li, X. Yin, C. Liu, X. Li, R. Ti, L. Fang, T. Zhang, R. Peng, and Y. Lu, "The nanoscale control of disorder-to-order layer-stacking boosts multiferroic responses in an Aurivillius-type layered oxide," J. Mater. Chem. C **9**(14), 4825–4837 (2021).

04 August 2025 15:15:43


© Author(s) 2025